Research Article | Vol. 28, No. 18 / 31 August 2020 / Optics Express 26492
Optics EXPRESS

Low-chirp push-pull dual-ring modulator with 144 Gb/s PAM-4 data transmission

XINRU WU,* BINBIN GUAN, QIANFAN XU, CHRIS DOERR, AND LONG CHEN

Acacia Communications, Inc. 101 Crawfords Corner Road, Holmdel, New Jersey 07733, USA
**xwu@acacia-inc.com*

Abstract: We experimentally demonstrate a low-chirp high-speed push-pull dual-ring modulator. The device is formed by two parallel cascaded add-drop ring modulators which has a Fabry-Perot resonance spectrally similar as electromagnetically induced transparency (EIT) effect. Differential drive signals are applied to the two rings to shift the individual resonances towards opposite directions, creating intensity modulation with suppressed frequency chirp. We present static and dynamic characterization of the device, including chirp parameter. We also demonstrate 144 Gb/s PAM-4 data transmission with 1-km standard single-mode fiber (SSMF) with BER below hard-decision forward error correction (HD-FEC) threshold with 7% overhead.

1. Introduction

The silicon microring modulator has emerged as a potential electro-optical modulator to provide a single-wavelength > 100 Gb/s data rate [1–5] for faster and energy-efficient optical interconnections in Data centers [6,7]. The microring modulator is preferable over other modulator structures because it can significantly reduce the device footprint of optical transmitters and can satisfy the evolving bandwidth and energy requirements [8]. However, there is a tradeoff between the optical bandwidth and modulation depth for a conventional microring modulator under a given drive voltage [9]. Furthermore, it is challenging to obtain chirp-free modulation with the conventional microring modulator [10,11]. A dual-ring configuration chirp-free modulator has been proposed theoretically in [12] and an experimental demonstration has been published recently [13], but only 10 Gb/s and 20 Gb/s OOK data transmission has been presented. However, a high-speed demonstration with over 100 Gb/s data transmission using this structure as well as experimental study of the chirp characteristic of this configuration has never been published yet.

In this article, we present a comprehensive experimental demonstration of a low-chirp, high-speed dual-ring modulator for PAM-4 transmission. It's low-chirp characteristic is experimentally demonstrated by measuring constellation diagrams using 5 GHz sine wave signals. The PAM-4 signals transmission at 144 Gb/s over 500-m and 1-km of standard single-mode fiber (SSMF) with bit error rates (BERs) below the hard-decision forward error correction (HD-FEC) threshold of 3.8×10^{-3} has been presented.

2. Dual-ring modulator design

For a typically single ring modulator, when the drive voltage is turned on/off, the resonance is shifted back and forth and thus the continuous wave (CW) laser light is modulated. In the optical domain, the modulation speed depends on how fast the light can be coupled in and out of the cavity, which is related to the photon lifetime and the resonance linewidth of the cavity. Hence increasing the coupling helps achieve a shorter photon lifetime and larger bandwidth. However, simply increasing the coupling will decrease the cavity Q and enlarge the resonator linewidth, which may either cause a lower extinction ratio in the modulated signals or require a larger resonance shift. Inevitably, there is a tradeoff between the bandwidth and resonance

#399800 https://doi.org/10.1364/OE.399800
Journal © 2020 Received 30 Jun 2020; revised 14 Aug 2020; accepted 16 Aug 2020; published 24 Aug 2020

Optics EXPRESS

shift for single ring modulator when keeping a certain extinction ratio. Instead, we describe a dual-ring modulator design shown in Fig. 1(a). The structure is formed by two rings which are coupled with two parallel bus waveguides, effectively forming a Fabry-Perot (FP) cavity with the two rings as mirrors, creating a resonance spectrally similar as the electromagnetically induced transparency (EIT) effect [12,14]. The EIT is in the atomic systems, due to quantum interference effects induced by coherently driving the atom with an external laser [15,16]. The transparency can also occur in a photonic resonator system by coherent interference between two coupled resonators [17]. In our design, two rings are identical and not coupled to each other directly. L_b is the waveguide distance between the centers of two rings. Integrated tunable optical phase shifters (TOPS) are placed on the two rings and the bus waveguide to control the resonances of the rings as well as the phase of the FP cavity. The EIT peak power changes with the relative resonance wavelengths shift of the two rings, which leads to an intensity modulation. The transmission of the center peak is enhanced by the FP cavity effect: i.e., small change in the mirror loss (drop-port transmission) can lead to large change in the overall FP transmission. So, the intensity modulation of the EIT peak is much more efficient than the pure index modulation which is used in the MZI push-pull configuration [10]. The frequency chirp of the modulated signals is eliminated as the two rings always shift in the opposite wavelength directions and thus the round-trip optical phase through two rings remain the same. With the push-pull drive, the modulation extinction ratio is enhanced compared to conventional single-ring modulators [13]. Figures 1(b) and (c) present the simulated transmission spectra and phase response of the dual-ring modulator with multiple cases of effective index differences between the two rings, which can be controlled by the differential driving voltages.

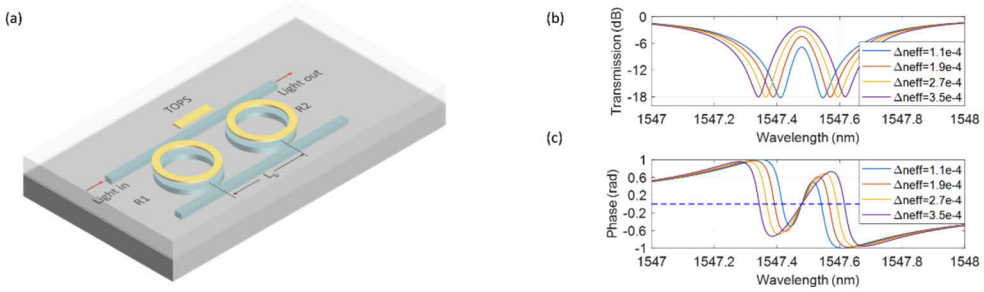

Fig. 1. (a)Schematic diagram of the dual-ring modulator. The yellow elements are the thermal optical phase shifters (TOPS); R1 and R2 correspond to ring1 and ring2; (b) Static transmission spectra and (c) phase responses of the dual-ring modulator under different index differences, that is different differential driving voltages.

It is known that ring modulator has peaking effect when the carrier wavelength detunes from the resonance wavelength, which can enhance the modulator bandwidth. However, it reduces the optical modulation amplitude (OMA). In this double ring structure, the push-pull structure will largely enhance the OMA while keeping the bandwidth enhancing benefit from the peaking effect. For different modulation format, different optimum DC bias points is needed. In our experiment, for the optimum PAM-4 modulation performance, the operation point is set for the FP resonance approximately 5.5 dB down from the maximum transmission point.

3. Dual-ring modulator characterization

Figure 2 shows the top-view microscope image of the fabricated device with grating couplers (GCs) for testing. The designed device was fabricated on a silicon-on-insulator (SOI) wafer with 220 nm silicon thickness. The radius for both microring modulators is 15 μm and the silicon waveguide has a width of 500 nm with a 90 nm slab. The nominal center-to-center distance

Optics EXPRESS

(the L_b shown in Fig. 1(a)) between the two rings is 140 µm. Three RF pads are designed as signal-ground-signal (SGS), with one signal driving each ring. Four DC pads are used to control the resonances of the two rings and the phase section between two rings (three for signals and one for common ground). During the measurements, the DC pads are probed by a DC probe card and the probe card is controlled by a NI Voltage Output Module (NI 9264). The DAC is programed by a Python script, which generates three different sliders to control the three output voltages with a step of 0.01Volts. Thus, during the measurement, we can move the slider to change the applied voltages on each TOPS. For optimum modulation performance, the operation point is set for the FP resonance approximately 5.5 dB down from the maximum transmission point. A testing device with the same nominal design which is expected to have the similar performance with the device under test is used for the DC characterization. The measured DC transmission spectra of the device are shown in Fig. 3(a). The total on-chip insertion loss is approximately 14 dB, including ~8 dB for the input and output grating couplers together. For each individual ring resonance (when the other ring resonance is tuned to far away), the extinction ratio is measured to be ~19 dB and the loaded Q factor is ~5000. Figure 3(a) shows the DC modulation efficiency for the dual-ring modulator. Figure 3(b) depicts the extracted transmission change (linear scale) at the operation wavelength λ_c (the transmission point at the dash line in Fig. 3(a)) versus applied push-pull voltages from Fig. 3(a). This means for this device the DC modulation efficiency is ~4.5 dB for 3 V voltage swing. Figure 4 presents the measured electro-optic (EO) S_{21} response. It shows a 3-dB bandwidth of this device is ~ 42 GHz at -4 V common bias, thanks to strong peaking at 25 GHz due to the offset between the laser frequency and ring resonant frequency. The EO bandwidth of the device is affected by two factors: first, the intrinsic EO bandwidth of the individual rings, which is determined by the resistance-capacitance characteristics of the junction and the optical quality factor; second, the peaking associated with detuning between

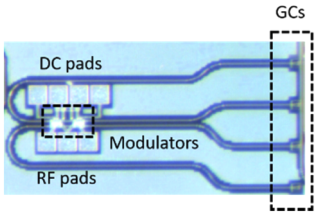

Fig. 2. Top-view microscope image of the fabricated device.

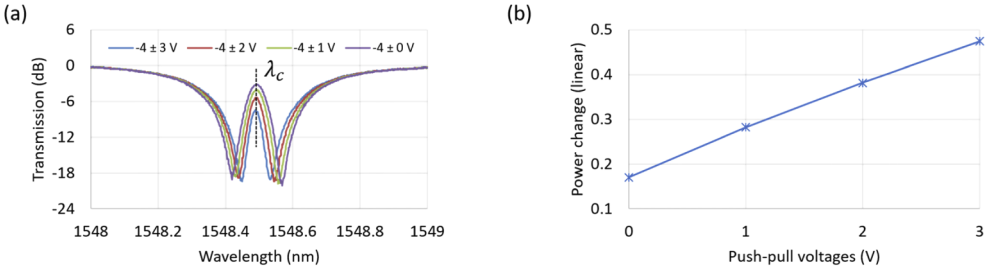

Fig. 3. (a) Measured transmission spectra when applying different reverse bias voltages on the RF pads. -4 volt is the common bias and the ± voltages are the push-pull voltages applied on the two rings, i.e. -4 ± 3 V correspond to -7 V bias on R1 and -1 V bias on R2. (b) The measured DC modulation efficiency at the EIT peak position when applying different push-pull voltages on the two rings.

Optics EXPRESS

the carrier frequency and the resonant frequency. A large detuning can boost the EO bandwidth while reducing the modulation efficiency.

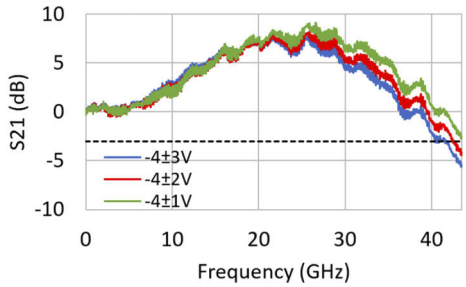

Fig. 4. Measured frequency response of the dual-ring modulator. -4 V common bias is used during the measurement with ±3 V, ±2 V and ±1 V push-pull voltages applied on the two ring modulators.

4. Chirp measurement and PAM-4 data transmission

We then characterized the modulator chirp parameter with large signal modulation. Figure 5 shows the experimental setup for the chirp measurement and PAM-4 data transmission. The chirp of both the dual-ring and single-ring modulator are evaluated by measuring the complex optical field with an Optical Modulation Analyzer (Keysight 4391A) while the modulators are driven with a 5 GHz sine wave to emphasize the modulation transitions.

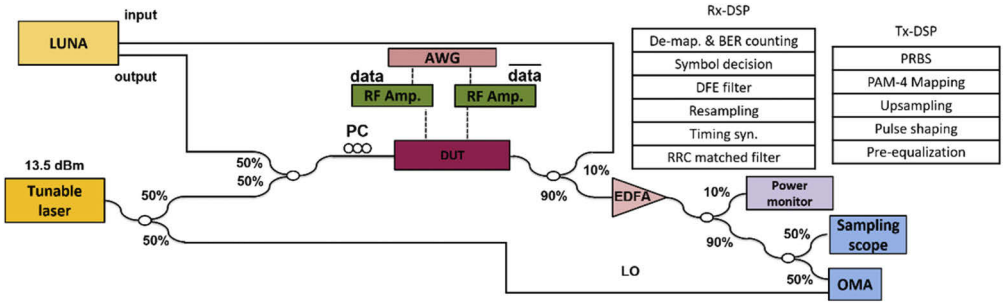

Fig. 5. Experimental setup for chirp characterization and PAM-4 data transmission. DSP: Digital Signal Processing, PRBS: Pseudo Random, Bit Sequence, BER: Bit Error Rate, DFE: Decision-feedback Equalizer, RRC: Root-raised-cosine, PC: Polarization Controller, DUT: device under test, AWG: Arbitrary Waveform Generator, LO: Local Oscillator, EDFA: Erbium-doped Fiber Amplifier

Figures 6(b) and (e) show the recovered optical field. For the dual-ring device, the transition between levels is straight, which confirms a negligible level of chirp, while the transition for a single-ring condition is significantly curved. Figures 6(a) and (d) present the time dependence of the optical intensity and phase. To quantify the chirp performance, we use an effective chirp parameter [18] defined as $\alpha_{3dB} = 2[\Phi(on) - \Phi(3dB)]/In[I(on)/I(3dB)]$, where $\Phi(on)$, $\Phi(3dB)$, $I(on)$, $I(3dB)$ are the phase and intensity at the 'on' state (100% transmission) and the '3dB' state (50% transmission). For the dual-ring push-pull drive case, the effective chirp parameter is 0.19, while for the single-ring device, the value is 1.26. It is obvious that the dual-ring configuration has much better chirp performance than the conventional single ring modulation. Figures 6(c) and (f) also show the 53 Gb/s OOK modulation for dual-ring and single-ring configurations. It

Optics EXPRESS

can be clearly seen that the modulation amplitude for the dual-ring device is much larger than the single-ring device. This further proves that the push-pull drive dual-ring modulator is beneficial for improving modulation amplitude.

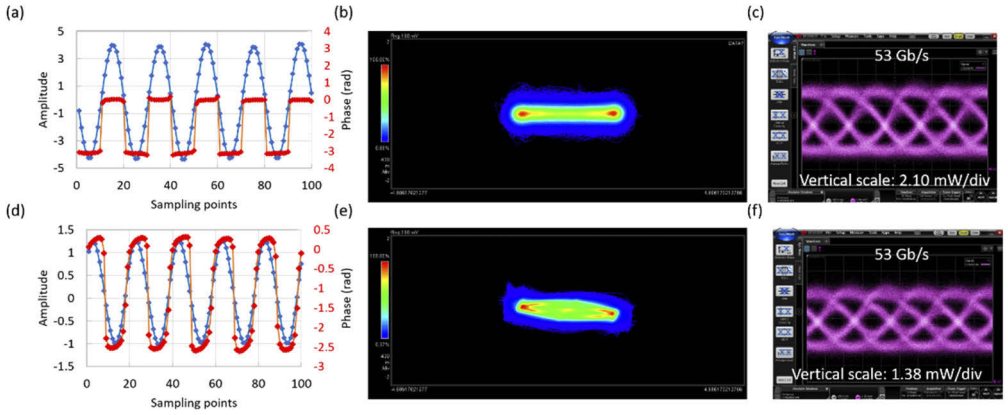

Fig. 6. Measured modulation chirp driving with a 5 GHz sine wave. (a) (b) (c) are for the dual-ring modulator and (d) (e) (f) are for the single-ring modulator. (a) (d) Captured amplitude and phase information of the electric field from optical modulation analyzer; (b) (e) real-time scope electric field waveforms and (c) (f) 53 Gb/s OOK signals of the dual-ring modulator and single-ring modulator.

Finally, we characterize the PAM-4 data transmission performance for the dual-ring push-pull modulator. The experimental setup and digital signal processing (DSP) flow are shown in Fig. 5. A tunable laser with 13.5 dBm output power is launched into the device with a wavelength located at ~1547 nm. The common bias of the two rings is -4 V with a push-pull voltage of ±1 V, i.e. R1 is biased at -5 V and R2 is biased at -3V. There are two reasons to use -4 V common bias. One is to guarantee both rings are operating at reverse bias region and another reason is to gain higher bandwidth with reasonably larger reverse bias. An optical vector network analyzer (LUNA) is used to monitor the carrier wavelength location versus the transfer function of the device during the data modulation. After the EDFA and before the photodetector, a narrow-band tunable filter is used to filter out the optical signal from the LUNA as well as the amplified spontaneous emission (ASE) noise from the EDFA. For practical use, the resonance frequencies for all resonators can be accurately aligned via active tuning. The differential electrical signals are generated by an arbitrary waveform generator (AWG) (Keysight M8196A) at 92-GSa/s. Then the electrical signals are amplified to ~2V peak-to-peak voltage by two individual RF amplifiers (SHF S807C) and then applied to the device through a GSGSG RF probe (GGB model 67A), landing on the SGS pads on the PIC (with two G tips on both sides floating). The modulated output signal is coupled out through a grating coupler and then amplified by an erbium-doped fiber amplifier (EDFA). A 50-GHz 3-dB bandwidth p-i-n photodiode (PD) without a trans-impedance amplifier (TIA) is used to convert the optical signal to the electrical signal. The electrical signal after the PD is captured by the real-time oscilloscope at 160-GSa/s.

The DSP stacks in Fig. 5 illustrate the sequential steps of the offline DSP used in this experiment. At the transmitter side, 72 Gbaud (144 Gb/s) PAM-4 signals are generated with Nyquist pulse shaping. An inverted linear filter-based pre-compensation is used to combat the channel fading. At the receiver side, a matched root-raised-cosine (RRC) filter is performed to mitigate the effects of white noise and then the received signals are resampled to two samples per symbol for the receiver-side equalization. Then a conventional decision-feedback equalizer (DFE) is applied to restore the signal. Finally, the output PAM-4 signal is decoded for bit error rate (BER) counting.

Optics EXPRESS

Figure 7(a) presents the BER performance of the 144 Gb/s PAM-4 signal versus the received optical power before the EDFA in the back-to-back (b2b), after 500-meter and 1-km SSMF transmission. The optimum BERs for b2b, 500-m and 1-km SSMF transmission are all below the hard-decision forward error correction (HD-FEC) coding limit, which has 7% overhead. The BER penalty of 1-km fiber transmission mainly comes from the fiber dispersion, because the chirp from modulator itself is negligible for this dual-ring configuration. Clearly open eye diagrams of the received 144 Gb/s PAM-4 signals at the largest received optical power are shown in Figs. 7(b) and (c) for each case.

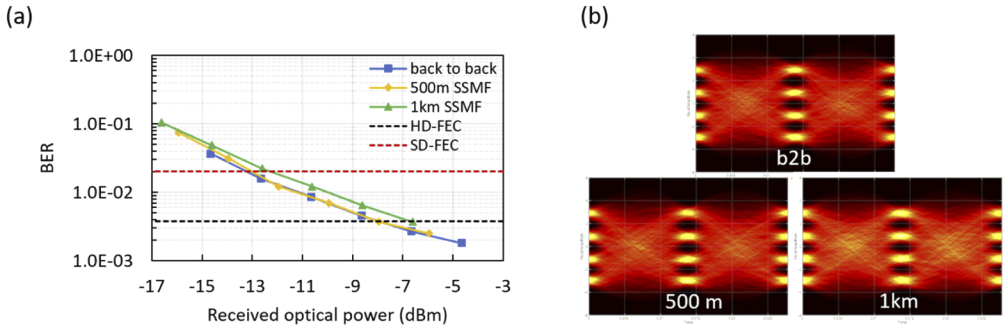

Fig. 7. (a) Measured offline BERs of the dual-ring modulator operating at 144 Gb/s data rate for back-to-back (b2b), after 500-m and 1-km standard single-mode fiber transmission; (b) the measured eye diagrams at the maximum received optical power for each case.

5. Conclusion

We experimentally demonstrated, to the best of our knowledge, the first silicon dual-ring modulator operating as high as 144 Gb/s data rate with a low chirp. PAM-4 transmission at 144 Gb/s over 500-m and 1-km SSMF is successfully demonstrated with BERs below the HD-FEC threshold of 3.8×10^{-3}. The frequency chirp of the modulated signals is considerably suppressed owing to the push-pull configuration, and push-pull results in a better modulation amplitude and being more power efficiency compared to single-ended drive with the same drive voltage.

Disclosures

The authors declare no conflicts of interest.

References

1. A. V. Krishnamoorthy, H. D. Thacker, O. Torudbakken, S. Muller, A. Srinivasan, P. J. Decker, H. Opheim, J. E. Cunningham, I. Shubin, X. Zheng, M. Dignum, K. Raj, E. Rongved, and R. Penumatcha, "From Chip to Cloud: Optical Interconnects in Engineered Systems," J. Lightwave Technol. **35**(15), 3103–3115 (2017).
2. J. Sun, R. Kumar, M. Sakib, J. B. Driscoll, H. Jayatilleka, and H. Rong, "A 128 Gb/s PAM4 Silicon Microring Modulator With Integrated Thermo-Optic Resonance Tuning," J. Lightwave Technol. **37**(1), 110–115 (2019).
3. H. Li, G. Balamurugan, M. Sakib, J. Sun, J. Driscoll, R. Kumar, H. Jayatilleka, H. Rong, J. Jaussi, and B. Casper, "A 112 Gb/s PAM4 Transmitter with Silicon Photonics Microring Modulator and CMOS Driver," in *Optical Fiber Communication Conference Postdeadline Papers 2019* (OSA, 2019), p. Th4A.4.
4. Y. Tong, Z. Hu, X. Wu, S. Liu, L. Chang, A. Netherton, C.-K. Chan, J. E. Bowers, and H. K. Tsang, "An Experimental Demonstration of 160-Gbit/s PAM-4 Using a Silicon Micro-Ring Modulator," IEEE Photonics Technol. Lett. **32**(2), 125–128 (2020).
5. X. Wu, C. Huang, K. Xu, C. Shu, and H. K. Tsang, "Mode-Division Multiplexing for Silicon Photonic Network-on-Chip," J. Lightwave Technol. **35**(15), 3223–3228 (2017).
6. R. Jones, P. Doussiere, J. B. Driscoll, W. Lin, H. Yu, Y. Akulova, T. Komljenovic, and J. E. Bowers, "Heterogeneously Integrated InP\/Silicon Photonics: Fabricating Fully Functional Transceivers," IEEE Nanotechnol. Mag. **13**(2), 17–26 (2019).

Optics EXPRESS

7. T. Shi, T.-I. Su, N. Zhang, C. Hong, and D. Pan, "Silicon Photonics Platform for 400G Data Center Applications," in *Optical Fiber Communication Conference* (OSA, 2018), p. M3F.4.
8. G. Li, A. V. Krishnamoorthy, I. Shubin, J. Yao, Y. Luo, H. Thacker, X. Zheng, K. Raj, and J. E. Cunningham, "Ring Resonator Modulators in Silicon for Interchip Photonic Links," IEEE J. Sel. Top. Quantum Electron. **19**(6), 95–113 (2013).
9. H. Yu, D. Ying, M. Pantouvaki, J. Van Campenhout, P. Absil, Y. Hao, J. Yang, and X. Jiang, "Trade-off between optical modulation amplitude and modulation bandwidth of silicon micro-ring modulators," Opt. Express **22**(12), 15178 (2014).
10. R. Li, D. Patel, E. El-Fiky, A. Samani, Z. Xing, M. Morsy-Osman, and D. V. Plant, "High-speed low-chirp PAM-4 transmission based on push-pull silicon photonic microring modulators," Opt. Express **25**(12), 13222 (2017).
11. L. Zhang, J.-Y. Yang, M. Song, Y. Li, B. Zhang, R. G. Beausoleil, and A. E. Willner, "Microring-based modulation and demodulation of DPSK signal," Opt. Express **15**(18), 11564 (2007).
12. X. Sun, L. Zhou, M. Jäger, D. Petousi, L. Zimmermann, and K. Petermann, "Silicon dual-ring resonator-based push-pull modulators," in G. T. Reed and A. P. Knights, eds. (2016), p. 975208.
13. D. Zheng, C. Qiu, H. Zhang, X. Jiang, and Y. Su, "Demonstration of a push-pull silicon dual-ring modulator with enhanced optical modulation amplitude," J. Lightwave Technol. **38**(14), 3694–3700 (2020).
14. Q. Xu, J. Shakya, and M. Lipson, "Direct measurement of tunable optical delays on chip analogue to electromagnetically induced transparency," Opt. Express **14**(14), 6463 (2006).
15. S. E. Harris, "Electromagnetically induced transparency," Phys. Today **50**(7), 36–42 (1997).
16. M. D. Lukin and A. Imamoglu, "Controlling photons using electromagnetically induced transparency," Nature **413**(6853), 273–276 (2001).
17. Q. Xu, S. Sandhu, M. L. Povinelli, J. Shakya, S. Fan, and M. Lipson, "Experimental Realization of an OnChip All-Optical Analogue to Electromagnetically Induced Transparency," Phys. Rev. Lett. **96**(12), 123901 (2006).
18. L. Chen, P. Dong, and Y.-K. Chen, "Chirp and Dispersion Tolerance of a Single-Drive Push–Pull Silicon Modulator at 28 Gb/s," IEEE Photonics Technol. Lett. **24**(11), 936–938 (2012).